Covalently conjugated polypyrrole-chitosan nanofibrous conductive composites prepared using dialdehyde polysaccharide linkers

Covalently conjugated polypyrrole-chitosan nanofibrous conductive composites prepared using dialdehyde polysaccharide linkers

Lukáš Münster[a,*], Monika Muchová[a], Martina Martínková[a], Věra Kašpárková[a,b], Petr Humpolíček[a,b], Jan Vícha[a]

[a]*Centre of Polymer Systems, Tomas Bata University in Zlín, tř. Tomáše Bati 5678, 760 01 Zlín, Czech Republic*

[b]*Department of Fat, Surfactant and Cosmetics Technology, Faculty of Technology, Tomas Bata University in Zlín, nám T. G. Masaryka 5555, 760 01 Zlín, Czech Republic*

**Corresponding author. E-mail address: munster@utb.cz (L. Münster).*

ABSTRACT

Polypyrrole (PPy) composites, despite their conductivity and bioactivity, are prone to degradation (e.g., exfoliation or delamination) due to the lack of chemical bonds between PPy and the matrix. Rather than suppressing this degradation through laborious methods involving toxic organic linkers or custom pyrrole derivatives to achieve covalently bonded PPy composites, this study introduces a novel polysaccharide-based approach. This method uses dialdehyde polysaccharides ($DAPs$) to conjugate PPy to chitosan nanofibers ($CHITs$) covalently. DAPs stabilize $CHITs$ through Schiff base chemistry and then conjugate pyrrole via aldol condensation. During subsequent polymerization, the conjugated pyrrole is incorporated into the PPy layer formed around the CHITs, covalently linking both polymers. The resulting composites exhibit good conductivity and cytocompatibility, making them promising for biomedical applications and tissue engineering. Moreover, this method is not limited to chitosan but can be extended to other amine-containing substrates.

Keywords: Chitosan nanofibers, dialdehyde polysaccharides, polypyrrole, conductive composite

1. Introduction

Polypyrrole (PPy) is a highly promising conductive polymer with considerable potential in various fields, including sensors [**1**], wearable electronics [**2**], battery electrodes [**3**], and water desalination [**4**]. The conductivity, ability to control cell differentiation [**5**], and good biocompatibility [**6**] also make it attractive for biomedical applications [**7**]. However, certain limitations have prevented the broad use of PPy and its composites.

First, there are environmental concerns. PPy is typically synthesized as thin films [**8**], powders [**9**], or colloidal dispersions [**10**] via the oxidative polymerization of pyrrole (py) in highly acidic solutions using potentially harmful oxidizing agents such as iron(III) chloride ($FeCl_3$) or ammonium persulfate. Although

green methods for PPy production are emerging, they are not yet ready for broader applications [**11**]. Thus, any improvement to the effectiveness of the current methods would be beneficial.

Second, neat PPy is brittle and difficult to process, which limits its applications. Consequently, various PPy composites have been used. These are commonly prepared by dispersing pre-made PPy powder in a polymer matrix or by initiating in situ polymerization of py within the matrix. Although straightforward, these approaches often yield heterogeneous materials with variable properties [**12**]. In addition, these composites are held together only by weak interactions such as hydrogen bridges or van der Waals forces. The absence of covalent bonds limits the adhesion between the PPy domains and the matrix, increasing the risk of PPy particle leaching or composite delamination.

To improve the properties of the PPy composites, two primary approaches are employed. The first method relies on electrostatic interactions between the negatively charged matrix and positively charged PPy [**13**], while the second relies on the covalent binding of py derivatives to the matrix, followed by in situ polymerization of PPy [**14,15**]. The former method is more prevalent because many matrices contain negatively charged groups or are easily modifiable for this purpose. Although the latter approach offers potentially more stable covalent bonds, it is significantly challenging. It often requires custom py derivatives, highly toxic linkers, or complex and environmentally harmful procedures [**15**]. These factors increase the synthesis cost and pose a risk of release of hazardous residues from the composite.

The preparation of PPy composites becomes even more challenging when a finely structured matrix is used. For instance, to prepare conductive nanofibrous composites, a continuous PPy layer must be generated in situ on the nanofibrous matrix to maximize the conductivity while preserving the shape of the underlying (nano)structure. This is particularly difficult with highly hydrophilic biopolymer nanofibers, which tend to swell or even dissolve under the harsh conditions required for PPy preparation (e.g., aggressive oxidizing agents, very low pH). The swelling of these matrices renders them highly sensitive to the PPy layer exfoliation due to the absence of strong interactions with the substrate.

Hence, we developed a novel approach utilizing an aldol condensation reaction [**16**] to prepare a well-defined 3D composite based on chitosan nanofibers ($CHITs$) with a PPy layer covalently bound using dialdehyde polysaccharides ($DAPs$). We also describe the reaction mechanisms and characterize the resulting composites in terms of their physicochemical properties and cytotoxicity in direct contact.

The entire approach (**Scheme 1**) begins with the periodate oxidation (POX) of the source polysaccharides to $DAPs$. In general, POX targets the vicinal hydroxyl groups of anhydroglucopyranose units, introducing a pair of reactive aldehyde ($-CHO$) groups per unit while disrupting the respective $C-C$ bond. This modification is considered sustainable because the periodate can be easily recovered [**17**]. The polysaccharides used in this study include cellulose, alginate, sodium hyaluronate, and dextran, which are oxidized to 2,3-dialdehyde cellulose (DAC), 2,3-dialdehyde alginate ($DAAL$), 2,3-dialdehyde hyaluronate (DAH), and dialdehyde dextran ($DADXA$) (see **Scheme 2** for structural formulae). Cellulose, the most abundant polysaccharide on Earth, is a key component of plant cell walls.

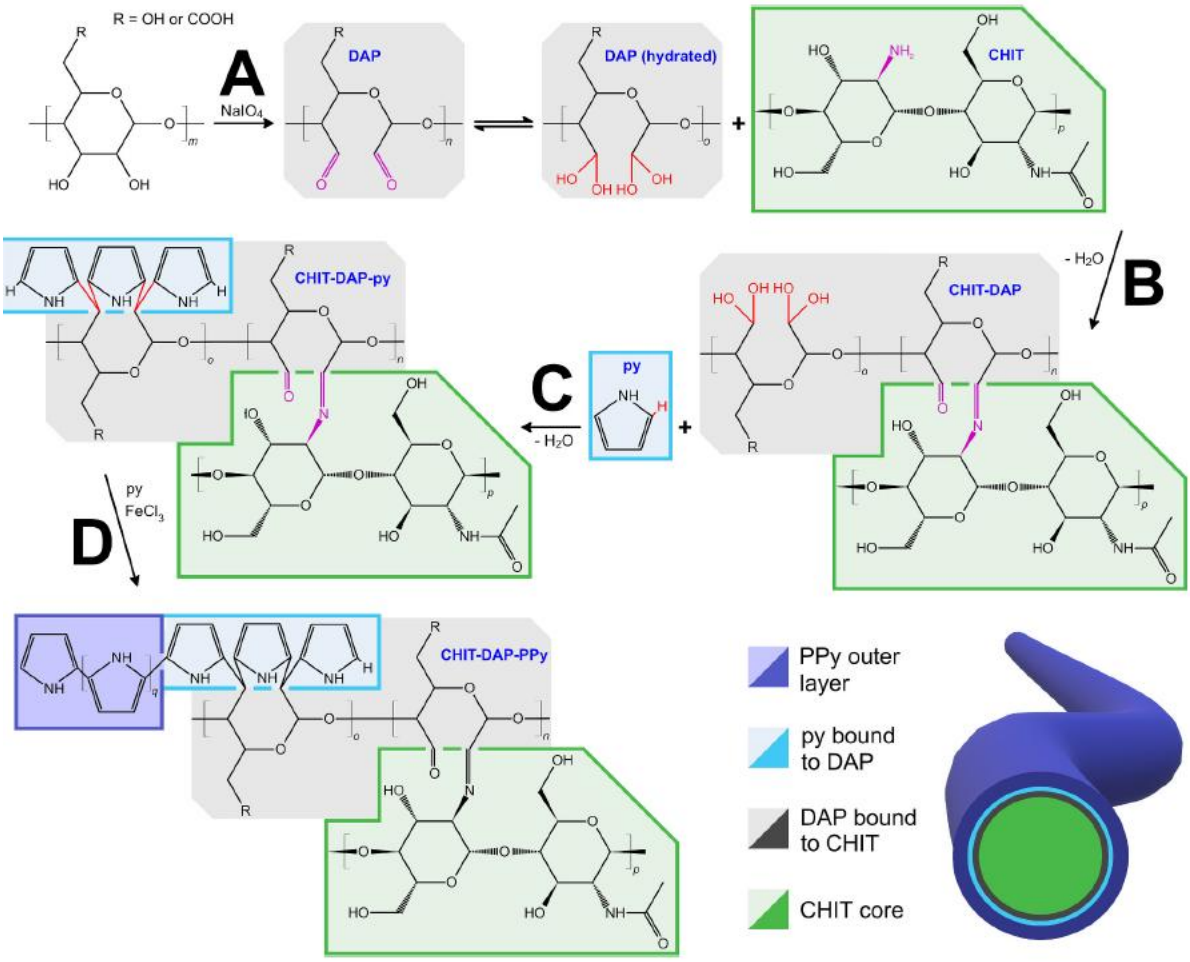

Scheme 1. Part A: Reaction scheme illustrating the periodate oxidation of polysaccharides containing vicinal hydroxyl groups, and their conversion into dialdehyde polysaccharides (DAP). Part B: Conjugation of DAP with chitosan nanofibers ($CHIT$) via a Schiff base reaction results in the formation of $CHIT-DAP$. Part C: Conjugation of $CHIT-DAP$ with pyrrole (py) via aldol condensation, yielding the $CHIT-DAP$-py conjugate. Part D: Subsequent growth of polypyrrole (PPy) on $CHIT-DAP-py$ in the presence of excess py and an oxidizing agent yielding $CHIT-DAP-PPy$ composite.

The structure of this compound comprises linear chains of anhydroglucose units linked by β-(1 → 4) glycosidic bonds. This arrangement results in a dense network of hydrogen bonds, rendering cellulose insoluble in water. However, cellulose can be chemically modified to form soluble derivatives, including solubilized DAC, which is an excellent crosslinker for various hydrogels [**18**]. Alginate is a natural polysaccharide extracted from brown algae. It consists of a linear chain of (1 → 4)-linked $\beta-D-$mannuronic acid and a-L-guluronic acid residues, forming a unique block structure. This structure allows alginate to form hydrogels upon exposure to divalent cations like calcium, making it versatile for various applications in food, pharmaceuticals, and biomedicine [**19**]. Alginate and cellulose are also important renewable resources with the potential to replace various fossil-based products [**20,21**]. Hyaluronic acid is a glycosaminoglycan composed of alternating D-glucuronic acid and N-acetyl-D-glucosamine units linked by β-(1 → 4) and β-(1 → 3) glycosidic bonds. Various tissues, including skin, cartilage, and synovial fluid, contain this polysaccharide, which plays crucial roles in cell migration, wound healing, and joint lubrication [**22**]. Dextrans are bacterial glycans linked by α-(1 → 6) glycosidic bonds with α-(1 → 3) branching. Produced by bacteria of the Leuconostoc and Streptococcus genera, dextrans are widely used in medicine as antithrombotic agents and plasma volume expanders [**23**].

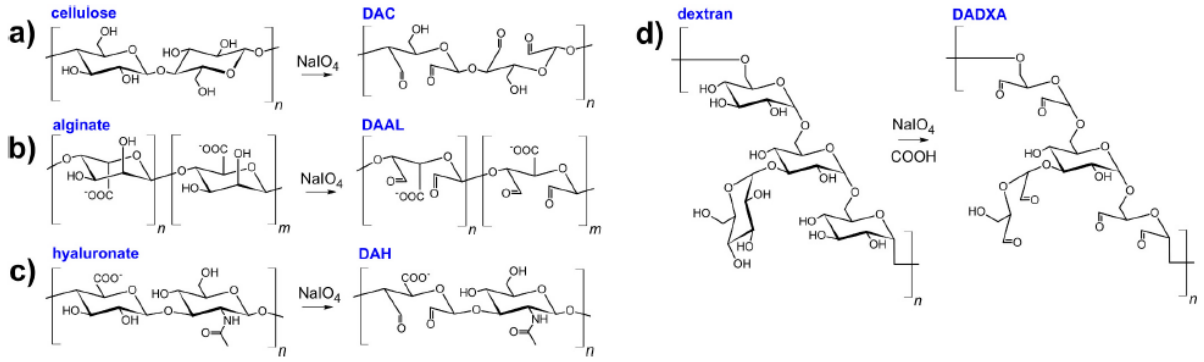

Scheme 2. Structures of selected polysaccharides and their periodate oxidized analogs.

$DAPs$ prepared from various polysaccharides then react with amine-rich $CHITs$ via a Schiff base reaction (**Scheme 1**, part B). The remaining —CHO groups of $DAPs$ are subsequently exposed to an excess of py, which spontaneously conjugates to the DAP layer via an aldol condensation reaction (**Scheme 1**, part C). The addition of $FeCl_3$ as an oxidizing agent then triggers the polymerization of py to PPy (**Scheme 1**, part D), whereas py conjugated to the DAP surface acts as the preferred substrate for the in situ growth of PPy. During this process, the py cycles bound to DAP are incorporated into PPy chains, creating covalent links and eliminating the need for specialized organic linkers. Thus, $DAPs$ act as "multifunctional linkers", firmly binding the underlying $CHITs$ substrate to the PPy. Furthermore, the crosslinking of chitosan chains by $DAPs$ protects the structure of $CHITs$ during the highly acidic polymerization of py and prevents their dissolution [**24**]. Because this research focuses primarily on nanofibrous composite preparation, a detailed study of the aldol condensation mechanism between $DAPs$ and py is beyond the scope of this study and will be covered in a subsequent contribution.

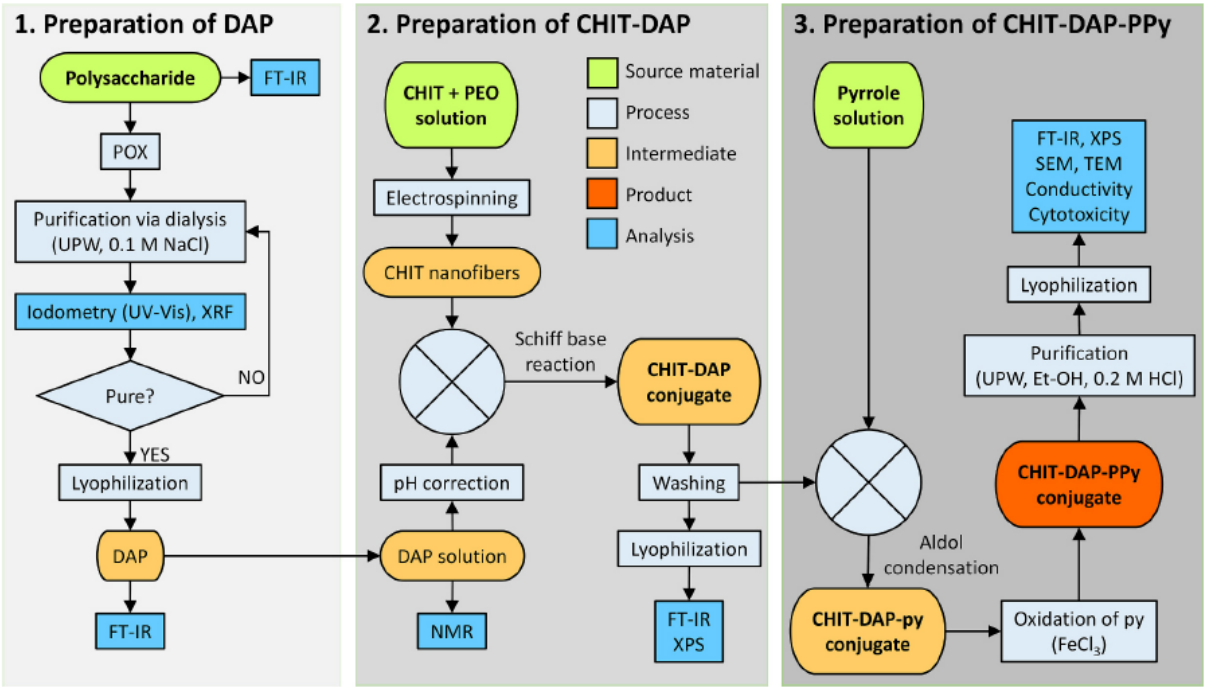

Scheme 3. Flowchart summarizing the experimental workflow, which is divided into sections detailing the three-step process for the preparation of $CHIT-DAP-PPy$ materials.

2. Materials and methods

To provide a clearer understanding of each step involved in the preparation and characterization of the composite, a flowchart of the experimental procedures is presented in **Scheme 3**.

2.1. Materials

Cellulose SigmaCell type 20 (Sigma Aldrich Co.) of weight-average molecular weight (M_w) = 76 kDa, dispersity (Đ) = 4.7, and degree of polymerization (DP) = 468; sodium alginate Protanal LF200S (FMC Biopolymer AS, Norway) with M_w = 250 kDa, fraction of guluronic acid (FG) = 0.68, and fraction of guluronic blocks (FGG) = 0.57; dextran from Leuconostoc spp. (Sigma Aldrich Co.) of M_w = 71 kDa, DP = 449, and Đ = 1.9; sodium hyaluronate of M_w= 1.5 MDa, DP = 3740, and Đ = 4.3 (Contipro Ltd., Czech Republic); sodium periodate ($NaIO_4$) (VWR, Czech Republic); sodium chloride ($NaCl$) (Penta, Czech Republic); potassium iodide (KI) (Penta, Czech Republic); potato starch (Sigma Aldrich Co.); hydroxylamine hydrochloride ($HAHCl$) (Sigma Aldrich); and hydrochloric acid (HCl, 35 %) (Penta, Czech Republic) were used for the preparation and characterization of $DAPs$. Medium molecular weight chitosan with M_w = 290 kDa, Đ = 6.7, and 78 % degree of deacetylation (Sigma Aldrich Co.); acetic acid (CH_3COOH) (Sigma Aldrich Co.); and polyethylene oxide (PEO) (Sigma Aldrich Co.) with viscosity-average molecular weight (M_v) = 600 kDa were used for the electrospinning of $CHITs$. Pyrrole (py, 98 %) (Sigma Aldrich Co.); ethanol ($Et-OH$) (VWR, Czech Republic); and diluted HCl were used in the preparation of $DAP-py$ conjugates. Anhydrous iron(III) chloride ($FeCl_3$) (Penta, Czech Republic) was used for subsequent py oxidation. The cytotoxicity assessment was performed using a cultivation medium consisting of Dulbecco's Modified Eagle's Medium (Biosera, France); sodium hydrogen carbonate (Penta, Czech Republic), 10 % bovine calf serum (CS, mycoplasma-free) (Biosera, France); and 1 % of penicillin/strep-tomycin (Biosera, France). All used chemicals were of analytical purity (p.a.) and used as received without further purification. Ultra-pure water (UPW, resistivity 18.6 MΩ •cm) was used throughout the experiment.

2.2. Preparation of $DAPs$ and $CHITs$

2.2.1. Synthesis of $DAPs$

Different DAPs were prepared using POX of source polysaccharides. For this purpose, alginate, dextran, and sodium hyaluronate (1 g) were dissolved, and cellulose (1 g) was dispersed in 50 mL of UPW for 24 h at ambient temperature. Subsequently, a solution containing 1.2 × the molar excess of $NaIO_4$ relative to the molar amount of oxidized units was added to ensure almost quantitative oxidation. The $NaIO_4$ masses required were as follows: 1.65 g for cellulose, 0.67 g for sodium hya-luronate, 1.35 g for sodium alginate, and 3.35 g for dextran, based on previous studies [**25-27**]. The described POX methodology was chosen for its reliability and reproducibility. To achieve an almost quantitative degree of oxidation ($DO \approx 100$ %), the oxidation reactions were carried out at 30 °C in the dark for 72 h for cellulose and 24 h for the other polysaccharides. After oxidation, the prepared DAC suspension was purified using five cycles of centrifugation at 10000 RPM for 15 min (Multifuge X3R, Thermo Fisher Scientific, USA) and mechanical homogenization at 10000 RPM for 10 min (WiseTis HG-15D homogenizer, Witeg, Germany). The DAC was then solubilized at 80 °C in an oil bath for 2 h using a three-necked flask equipped with a magnetic stirrer, an external thermometer probe, and reflux. Following solubilization, the DAC sample was centrifuged and filtered using a 0.45 |im syringe filter. The solubilized DAC, along with the other prepared soluble DAPs (DAH, DAAL, and DADXA), was dialyzed using 14 kDa molecular

weight cut-off (MWCO) dialysis tubing. Dialysis was performed against UPW (72 h), followed by 0.5 M NaCl (48 h), and then again against UPW (24 h) to remove salt. The purified DAP solutions were filtered (0.45 im) and lyophilized. The yields were 56 % for DAC, 74 % for DAAL, 99 % for DADXA, and 71 % for DAH.

2.2.2. Preparation of $CHITs$

$CHITs$ were prepared from a 20 mg/mL solution of chitosan in 70 % acetic acid containing PEO as a fiber-forming additive (weight ratio of chitosan: PEO = 5:1). The mixture, with a dynamic viscosity of 1.65 Pa•s and conductivity of 869 μS/cm, was filtered using a 1 μm glass syringe filter, degassed, and electrospun using a SpinLine 40 device (SPUR a.s., Czech Republic). The following parameters were used: flow rate = 0.15 mL/min, accelerating voltage = 60 kV, humidity = 25 %, working distance = 21 cm, cycle duration = 60 min, and polypropylene as the substrate.

2.3. Screening and synthesis of CHIT-DAP-PPy composites

2.3.1. Initial $CHIT-DAC-PPy$ screening

The influence of different amounts of py on the properties of the resulting $CHIT-DAC-PPy$ composite properties was initially investigated. $CHITs$ specimens measuring 1 × 1 cm (m = 1.9 mg) were cut, and the molar amount of — NH_2 groups ($n_{\_NH2}$) per specimen was calculated ($n_{\_NH2}$= 4.58 mmol/g in 78 % deacetylated chitosan). These $CHITs$ specimens were placed in 5 mL of a pH 6.5 solution containing 0.718 mg of dissolved DAC. This value corresponds to the molar amount of — CHO groups required to fully react with the — NH_2 groups on the $CHITs$ via a Schiff base reaction. The $CHITs$ specimens were left to react with DAC for 4 h to form imine bonds. Next, the $CHIT-DAC$ samples were removed from the DAC solution, gently washed to remove unbound DAC, and placed in solutions containing varying amounts (0 to 1000 mol%) of py relative to the $n_{\_CHO}$, i.e., the molar amount of — CHO groups in DAC solution used for conjugation with chitosan. These mixtures were gently shaken at ambient temperature in the dark for 16.5 h to allow aldol condensation between $DAC's$ — CHO groups and py (see **Scheme 1**, part C). Subsequently, 1 mL of a solution containing 4 × the molar amount of the oxidizing agent $FeCl_3$ relative to the used py was added dropwise to the $CHIT-DAC-py$ mixture to initiate the oxidation of py to PPy. This oxidation reaction was monitored for 4 h and then terminated by removing the $CHIT-DAC-PPy$ samples, which were washed in UPW, 0.2 M HCl, UPW, Et-OH, and UPW using an ultrasonic bath. After washing, the thin composite sheets were lyophilized and analyzed by SEM. In addition to the $CHIT-DAC-PPy$ samples, one blank sample ($CHIT-PPy\_$-blank) was prepared without DAC. **Table 1** summarizes the compositions of the reaction mixtures used in this experiment.

2.3.2. Synthesis of $CHIT-DAP-PPy$ composites

Based on the initial $CHIT-DAC-PPy$ experiment, three additional $CHIT-DAP-PPy$ materials were prepared using the same reaction conditions employed for $CHIT-DAC-PPy$200. These included $CHIT-DAAL-PPy$200, $CHIT-DADXA-PPy$200, and $CHIT-DAH-PPy$200. For conductivity analysis, $CHIT-DAC-PPy$200 and $CHIT-DAAL-PPy$200 were synthesized in bulk using an upscaled procedure with 100 mg of $CHITs$. After purification (removal of residual unbound PPy), these materials were mechanically homogenized, soaked in 0.2 M HCl for five days to protonate

the nonconducting PPy bases into conducting PPy salts and pressed into pellets with a diameter of 15 mm for conductivity measurements.

2.4. Characterization of $DAPs$, $CHITs$, and $CHIT-DAP-PPy$

2.4.1. Infrared spectroscopy ($FT-IR$)

Qualitative spectral analyses of the prepared $DAPs$ and $CHIT-DAP-PPy$ were performed using an $FT-IR$ spectrometer Nicolet 6700 (Thermo Fisher Scientific, USA) equipped with a diamond crystal in ATR mode, covering wavenumbers ranging from 4000 to 600 cm^{-1}.

2.4.2. Determination of degree of oxidation (DO)

The prepared $DAPs$ were characterized in terms of their DO using an oxime reaction followed by alkalimetric titration. Briefly, each DAP was dissolved in 30 mL of UPW (0.33 wt%), and the pH was adjusted to 4.0 with diluted HCl. Next, 20 mL of HAHCl solution (2.15 wt%, pH adjusted to 4.0) was added, and the mixture was gently stirred for 24 h. The consumption of 0.1 N NaOH was used to determine the aldehyde-to-oxime conversion and subsequent DO calculation [**28**]. The statistical analysis of the significance of differences in the obtained DO results was performed using one-way ANOVA with a post hoc Tukey's Multiple Comparison test ($p < 0.001$).

Table 1 The reaction conditions of the initial $CHIT-DAC-PPy$ experiment with varying amount of py and $FeCl_3$.

#	m CHITs (mg)	m DAC (mg)	py to n_{-CHO} (mol%)	V py (µL)	n py (µmol)	m $FeCl_3$ (mg)
CHIT-DAC-PPy0	1.9	0.718	0	0	0	0
CHIT-DAC-PPy10	1.9	0.718	10	0.12	1.80	1.16
CHIT-DAC-PPy50	1.9	0.718	50	0.62	8.97	5.82
CHIT-DAC-PPy200	1.9	0.718	200	2.49	35.89	23.29
CHIT-DAC-PPy500	1.9	0.718	500	6.23	89.72	58.22
CHIT-DAC-PPy1000	1.9	0.718	1000	12.45	179.46	116.43
CHIT-PPy_blank	1.9	0	–	2.49	35.89	23.29

2.4.3. Iodometry and $UV-Vis$ analysis

To evaluate potential contamination with residual iodine originating from POX, iodometry and subsequent $UV-Vis$ analysis of the prepared DAPs were performed. In a typical experiment, 2.5 mL of 10 mg/mL DAP solution was mixed with 0.5 mL of 5 % KI solution, 0.5 mL of 1 M HCl solution, and 0.5 mL of 2 % potato starch solution. After macroscopic evaluation, the mixture was transferred to a quartz cuvette and analyzed using a double-beam $UV-Vis$ spectrometer Lambda 1050 (PerkinElmer, USA) across wavelengths ranging from 250 to 800 nm.

2.4.4. X-ray fluorescence spectroscopy (XRF)

To further confirm the high purity of the $DAPs$ and the absence of iodine, XRF analysis was conducted using an energy-dispersive X-ray fluorescence spectrometer ARL Quant'X EDXRF Analyzer (Thermo Fisher Scientific, USA). Calibration standards were prepared by dissolving a defined amount of KI in UPW.

2.4.5. Nuclear magnetic resonance (NMR)

The ^{1}H NMR spectra of the source chitosan and $DAPs$ were recorded at a 10 mg/mL concentration using a JEOL 400 MHz NMR spectrometer (JEOL, Japan). Measurements were conducted at 298 K in a D_2O/DCl (0.1 M) mixture. The degree of acetylation of chitosan was determined based on Kasaai et al. [**29**], by comparing 1/3 of the signal intensity of CH_3(N-ac) to 1/6 of the sum of H2-H6 intensities.

2.4.6. X-ray photoelectron spectroscopy (XPS)

XPS analyses were carried out to investigate the binding interactions between $CHITs$, DAC, and PPy. An Axis Ultra DLD spectrometer (Kratos Analytical, UK) equipped with a monochromatic Al Ka (hv = 1486.7 eV) X-ray source operated at 75 W (5 mA, 15 kV) was used. The spectra were obtained using an analysis area of approximately 300 × 700 |im. The Kratos charge neutralizer system was used for all analyses. High-resolution spectra were recorded at a step size of 0.1 eV and a pass energy of 20 eV. The instrument base pressure during the measurements was consistently 2 × 10_8 Pa. The spectra were analyzed using CasaXPS software (version 2.3.15) and charge-corrected to the main line of the carbon C 1s spectral component ($C—C$, $C—H$) set to 285.0 eV. A standard Shirley background was applied to the sample spectra.

2.4.7. Scanning electron microscopy (SEM)

Images of the $CHIT-DAP-PPy$ samples were obtained using a Nova NanoSEM 450 microscope (FEI, Czech Republic) operated at an accelerating voltage of 5 kV. The samples were sputtered with gold-palladium nanoparticles to suppress the charge accumulation effect.

2.4.8. Transmission electron microscopy (TEM)

A JEM-2100 transmission electron microscope (JEOL, Japan) operated at an acceleration voltage of 160 keV was used for sample imaging. Diluted $CHIT-DAP-PPy$ dispersions were sonicated using an ultrasonic homogenizer Sonopuls HD 2070 with an MS 73 micro tip (Bandelin, Germany), drop-cast onto a 300-mesh copper grid coated with a For-mvar membrane, and gently dried.

2.4.9. Conductivity

The neat $CHITs$ and selected $CHIT-DAP-PPy$ samples ($CHIT-DAC-PPy$200 and $CHIT-DAAL-PPy$200) were analyzed for their conductivity (c). These samples were prepared in bulk and pressed into pellets with diameters of 15 mm and ∼2 mm thickness. Conductivity measurements were

performed using a programable electrometer Keithley 6517B (Textronix, USA) using the following equation (Eq. **1**):

$$\sigma = \frac{I}{U}\frac{t}{S} \quad (1)$$

Here t is the thickness of the sample, S is the surface area of the sample, and U and I are the voltage and current, respectively.

2.4.10. Cytotoxicity

Cytotoxicity assessment followed the ISO 10993 protocol. The cultivation conditions were maintained at 37 °C under a 5 % CO_2 atmosphere in humidified air using a HERAcell 150i incubator (Thermo Scientific, USA). Mouse embryonic fibroblasts (NIH/3T3 cells) were precultivated in 24-well plates (TPP, Switzerland) at a seeding density of 1×10^5 cells/mL of medium. Sterilized samples were subsequently added to cells for 24 h, and each sample was tested in quadruplicate. Cell viability after exposure was determined by the MTT assay using a Tetrazolium MTT cell proliferation assay kit (Duchefa Biochemie B. V., Netherlands). The absorbance was measured at 570 nm using an Infinite M200 Pro NanoQuant (Tecan, Switzerland), with a reference wavelength of 690 nm. Results are expressed as percentages of cell viability in NIH/3T3 cultures relative to the reference cells. A cell viability below 0.7 was considered the threshold for cytotoxicity according to ISO 10993-5. The statistical significance of the cytotoxicity results was determined by one-way ANOVA with a post hoc Tukey's Multiple comparison test ($p < 0.001$).

3. Results and discussion

3.1. Synthesis and characterization of DAP

POX is possible only for polysaccharides that contain at least one pair of vicinal — OH groups within their structural units. As described in the Introduction, this selective oxidation reaction results in the formation of two highly reactive — CHO groups, accompanied by the cleavage of the corresponding carbon-carbon bond. Although every unit of cellulose and sodium alginate can, in principle, be oxidized, (see **Scheme 2**, parts a and b) [**26,30**], N-acetyl-D-glucosamine units of sodium hyaluronate are resistant to POX (**Scheme 2**, part c) [**31**]. It is also worth noting that when several pairs of vicinal — OH groups are present within a structural unit, multiple oxidation can occur. This situation occurs in dextran's a-(1 → 6)-linked units, where three neighboring — OH groups are found at C2, C3, and C4. According to previous NMR analyses [**25,32**], the dextran used also contains approximately 15 % of α-(1 → 3)-branched units, which are resistant to POX. Consequently, the "complete" oxidation of dextran results in the elimination of C3 in the form of formic acid for a-(1 → 6)-linked units, while α-(1 → 3)-branched dextran units remain unaltered, as shown in **Scheme 2**, part d. The oxime reaction revealed the DO of the prepared $DAPs$ as follows: DAC 96.1 $\pm$ 0.5 %, 99.0 ± 0.3 %, $DAAL$ 96.0 $\pm$ 0.4 %, and DADXA 84.5 $\pm$ 0.4 %. One-way ANOVA with a post hoc Tukey's Multiple Comparison test with a post hoc Tukey's Multiple Comparison test ($p < 0.001$) showed statistically significant differences in DO between DAC and DAH, DAC and DADXA, DAH and $DAAL$, DAH and $DADXA$, and $DAAL$ and $DADXA$ (see Table S1 in Supplementary Information, SI). These differences can be attributed to the previously mentioned variations in supramolecular features (linear versus branched architecture), charge (anionic or neutral nature), and structural unit composition (heteropolysaccharide versus

homopolysaccharide). Conversely, the lack of a statistically significant difference between DAC and $DAAL$ is likely due to their shared linear backbone structure.

Fig. 1 shows the $FT-IR$ analysis of the unmodified source polysaccharides and their oxidized analogs (for full IR spectra, see Fig. S1 in SI). Typical motifs appearing in the IR spectra of all prepared $DAPs$ include (i) a $C=O$ vibrational band around 1730 cm^{-1}, which can be assigned to the $-CHO$ groups of the DAP, and (ii) an increase in the intensity of the $C-O-C$ vibrational band at 885 cm^{-1} in the DAC IR spectrum, signifying the formation of intermolecular hemiacetal structures between C6' and C2/C3 of DAC units [**26**]. The strong absorption around 1600 cm^{-1} ($C-O$ stretching of carboxylate anion) in the IR spectra of DAH and $DAAL$ samples is attributed to the carboxyl groups present in the source polysaccharides.

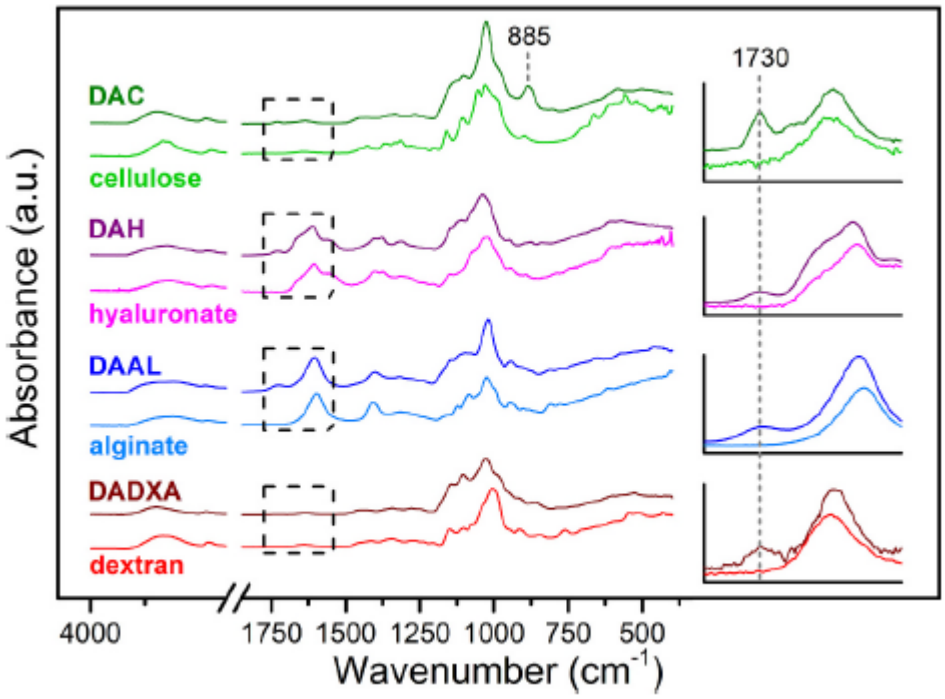

Fig. 1. $FT-IR$ analysis of the source polysaccharides and their periodate oxidized analogs. Full IR spectra are shown in Fig. S1 in SI.

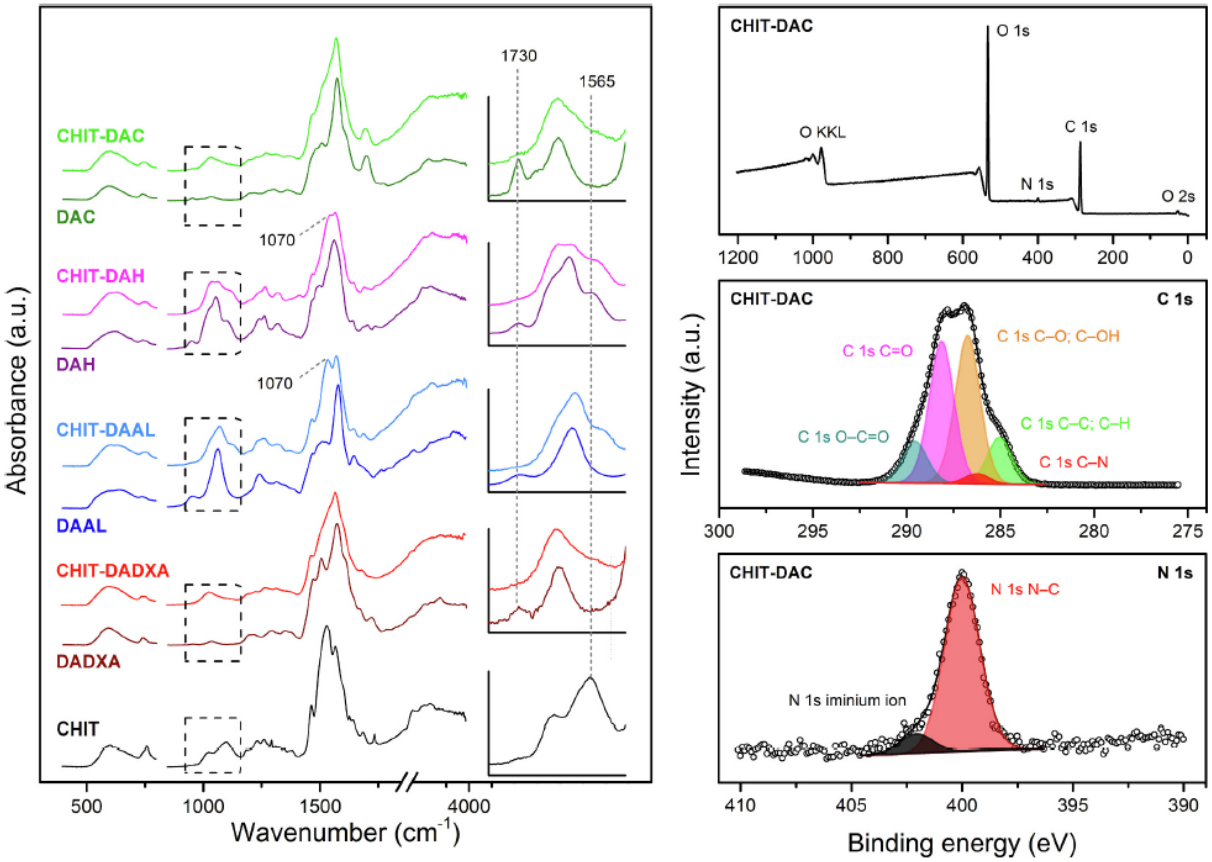

Fig. 2. FT-IR analysis of the prepared $DAPs$ and their conjugation with chitosan (left part) and XPS survey spectrum and high-resolution C 1s and N 1s scans obtained on the $CHIT-DAC$ sample. For full IR spectra, see Fig. S5 in SI.

Subsequently, iodometric titration and XRF analysis were performed to investigate the presence of residual iodate in $DAPs$ after POX. The residues of oxidizing agents are undesirable because they can react with py. The iodometric titration did not show any traces of iodine compounds, as evidenced by the absence of the triiodide/starch complex absorption band at around 600 nm in $UV-Vis$ spectra of the acidified DAP solutions (Fig. S2a). Furthermore, no traces of iodine were detected by XRF analysis (Fig. S2b). The ^{1}H NMR spectra of the $DAPs$ are presented in Fig. S3.

3.2. $CHIT-DAP$ synthesis and characterization

Prepared $DAPs$ were used to react with — NH_2 groups of the $CHITs$, crosslinking their surface and forming a thin reactive layer. The degree of deacetylation of the used chitosan was 60 %, as determined by NMR analysis (see Fig. S4). $FT-IR$ analysis confirmed the binding of $DAPs$ to the $CHITs$ surface (see left part of **Fig. 2**; for full IR spectra of $CHIT-DAPs$, refer to Fig. S5). All IR spectra of the prepared $CHIT-DAPs$ materials show a decrease in the intensity of the 1565 cm^{-1} band compared to the neat $CHITs$ spectrum (i.e., $N—H$ bending vibration originating from amine groups of $CHITs$), evidencing the binding of $DAPs$' $—CHO$ groups to the — NH_2 groups of $CHITs$ via Schiff base reaction, as proposed in the top and middle rows of **Scheme 1**.

To further analyze the binding between $DAPs$ and $CHITs$, XPS analysis was conducted on the $CHIT-DAC$ sample. **Fig. 2** (right part) displays the XPS survey spectrum and high-resolution C 1s and N 1s scans of the $CHIT-DAC$. The C 1s signal is composed of several peaks attributed to $C—C$ and $C—H$

bonds (285.04 eV, DAC, and $CHITs$), $C\text{—}N$ (286.23 eV, CHITs), C—O and C-OH (286.74 eV, DAC, and $CHITs$), $C\text{—}O$ (288.13 eV, aldehydes of DAC and $CHITs$ acetal groups), and $O-C=O$ (289.23 eV, probably from residual acetate from $CHITs$ preparation). The key evidence of the Schiff base reaction between $CHITs$ and DAC is exemplified in the bottom XPS spectrum, showing a high-resolution N 1s scan with the presence of an iminium ion signal (402.04 eV). Iminium-ion bonds are formed by the protonation of the imine group below their pKa. As no reducing agent was used to convert the iminium bonds between the DAC and $CHITs$ (i.e., no reductive amination was performed), the iminium bonds remained in the conjugate. The prepared $CHIT-DAP$ samples were then used to prepare the PPy composites.

3.3. $CHIT-DAP-PPy$ composite synthesis and characterization

Initially, $CHIT-DAC$ samples were shaken overnight in the presence of various amounts of py (**Table 1**), allowing aldol condensation to occur. For more details on aldol condensation between DAP and PPy, see our previous work [**16**]. The polymerization of py was subsequently initiated by the addition of $FeCl_3$. The resulting materials were thoroughly analyzed using the methods described in section 2.4. **Fig. 3** shows SEM micrographs of the prepared samples (left) illustrating the surface morphology changes and the dimensions of the nanofibers and composites. Inset photographs of the reaction vessels depict the progress of $CHIT-DAC-PPy$ formation after 15 min and 4 h of py oxidation.

Although no changes in the nanofibrous structure of $CHIT-DAC$ were observed for the $PPy0$ sample (i.e., without added py), the differences in surface morphology and nanofiber diameter, along with the color change of the samples, became evident as the concentration of py increased. These changes indicate the formation of a thin PPy layer in the $CHIT-DAC-PPy50$ sample. The growth of the PPy layer on the $CHIT-DAC$ surface is readily observable by SEM for samples prepared with ≥200 mol% of py relative to $n_{\_CHO}$ of DAC. This was accompanied by a more than two-fold increase in the nanofiber diameter, as summarized in the SEM analysis in **Fig. 3**. Notably, in the $CHIT-DAC-PPy200$ sample, PPy preferentially grows on the surface of $CHIT-DAC$, while the surrounding solution remains largely clear (see inset photographs in **Fig. 3**). This is likely due to py bound to the DAC providing an optimal substrate for PPy deposition. In contrast, samples prepared with py concentrations of 500 and 1000 mol% exhibit excessive PPy flakes formation throughout the reaction mixture (see inset photographs marked by green arrows in **Fig. 3**). This was likely due to the saturation of the $CHIT-DAC$ surface and the high py concentration. Unsurprisingly, PPy grains on $CHIT-DAC$ surfaces also became larger (from ~60 to 150 nm) as the py concentration increased from 500 to 1000 mol%.

To better illustrate the advantages of our approach, the entire procedure was repeated with neat $CHITs$ ($CHIT-PPy_$blank sample). The reaction conditions were identical to those for the $CHIT-DAC-PPy200$ sample, except that DAC was excluded (see **Table 1**). The experimental results were remarkably different. The $CHIT-PPy_$blank sample showed immediate swelling, followed by partial dissolution after 4 h (see bottom left part of **Fig. 3**). This behavior is a direct consequence of chitosan's solubility in acidic media, as the pH of the reaction mixture was ~2. Instead of a nanofibrous composite, the $CHIT-PPy_$blank sample consisted of a sheet-like material densely covered with PPy, as evidenced by SEM analysis. Thus, the preparation of $CHIT-PPy$ composites is not feasible without DAC.

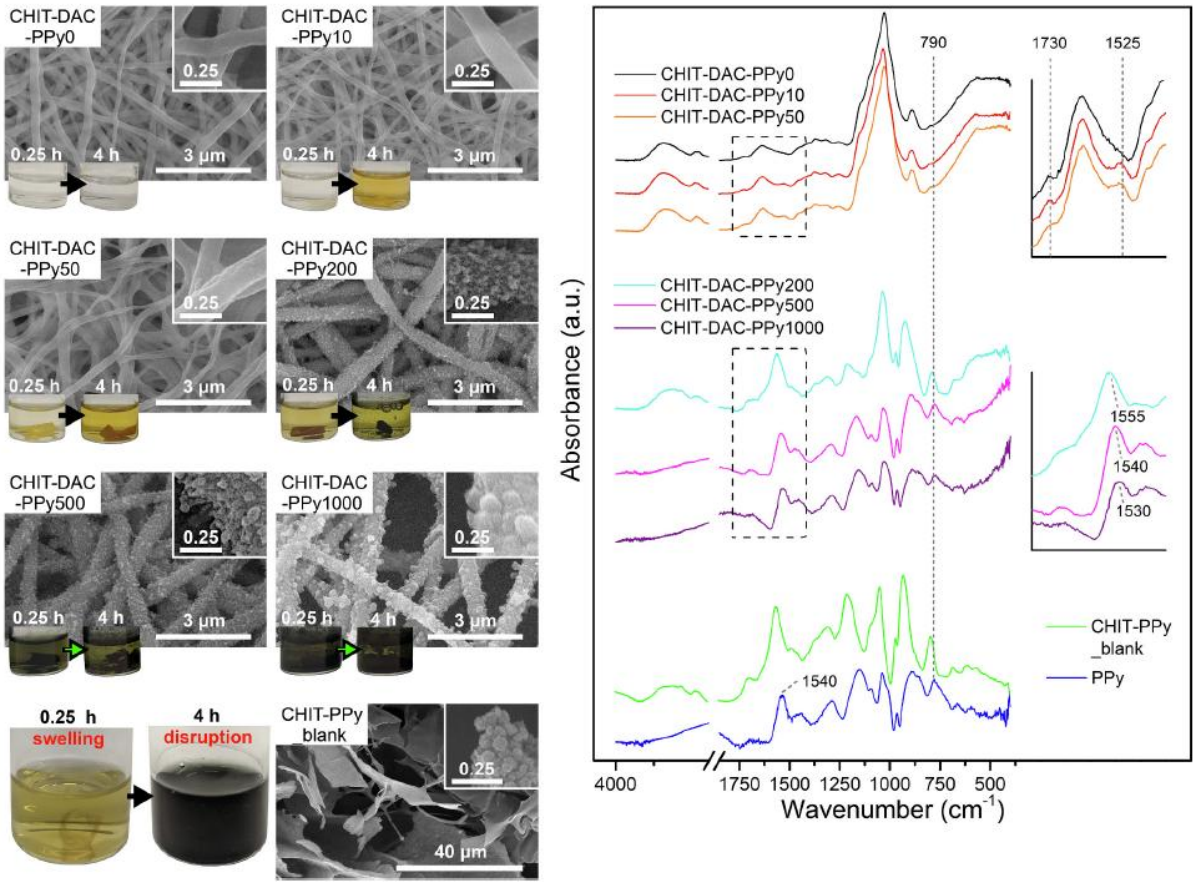

Fig. 3. SEM analysis of $CHIT-DAC$ conjugates and $CHIT-PPy$_blank (bottom left row) exposed to different amounts of py in the presence of $FeCl_3$, accompanied by inset photographs depicting the state of conjugation after 0.25 and 4 h (left part); $FT-IR$ analysis of the prepared $CHIT-DAC-PPy$ materials, $CHIT-PPy$_blank, and neat PPy, featuring magnified regions of interest with marked wavenumbers.

The right side of **Fig. 3** shows the IR spectra of $CHIT-DAC-PPy$ samples, the $CHIT-PPy$_blank sample, and the neat PPy prepared without support. When comparing the IR spectra of the $CHIT-DAC-PPy0$ sample (prepared without adding py) to those of the $CHIT-DAC-PPy10$ and $CHIT-DAC-PPy50$ samples, the appearance of vibration of the py cycle at 1525 cm^{-1} is evident. This indicates the presence of py oligomers or a thin layer of PPy, unobservable by SEM. There is also a noticeable increase in the intensity of the absorption band at ~790 cm^{-1} ($C—H$ out-of-plane deformational vibration of PPy). Further increase in the py concentration (≥200 mol%) resulted in considerable changes in the IR spectra, which resembled that of neat PPy. The strong increase in the $C—C$ stretching vibration intensity of PPy in the region from 1530 to 1555 cm^{-1} is particularly visible (see magnified detail in **Fig. 3**).

Based on the obtained data, $CHIT-DAC-PPy200$ was selected as the most promising sample and further analyzed by XPS (see **Fig. 4**). The XPS survey spectrum, along with the high-resolution C 1s and N 1s scans of $CHIT-DAC-PPy200$, are presented. The presence of PPy was reflected in the XPS survey spectrum (top row) by a comparatively stronger N 1s signal than in the XPS survey spectrum of the $CHIT-DAC$ conjugate (**Fig. 2**). Chlorine residues are likely due to washing with hydrochloric acid. The high-resolution C 1s scan (middle row of **Fig. 4**) shows peaks associated with DAC and $CHITs$ bonding, as described in the first paragraph of section 3.2. Additionally, a newly formed signal at 284.13 eV (C 1s C=C) and a significant increase in the intensity of the signal at 286.09 eV (C 1s $C—N$) indicate the presence of PPy. The high-resolution N 1s scan (bottom row) reveals

three signals: 400.04 eV (N 1s N— C) from the amino groups of $CHITs$', 401.79 eV (N 1s iminium ion) from covalent interactions between $CHITs$ and DAC, and 398.16 eV (N 1s $R = N$— C) from aromatic PPy cycles.

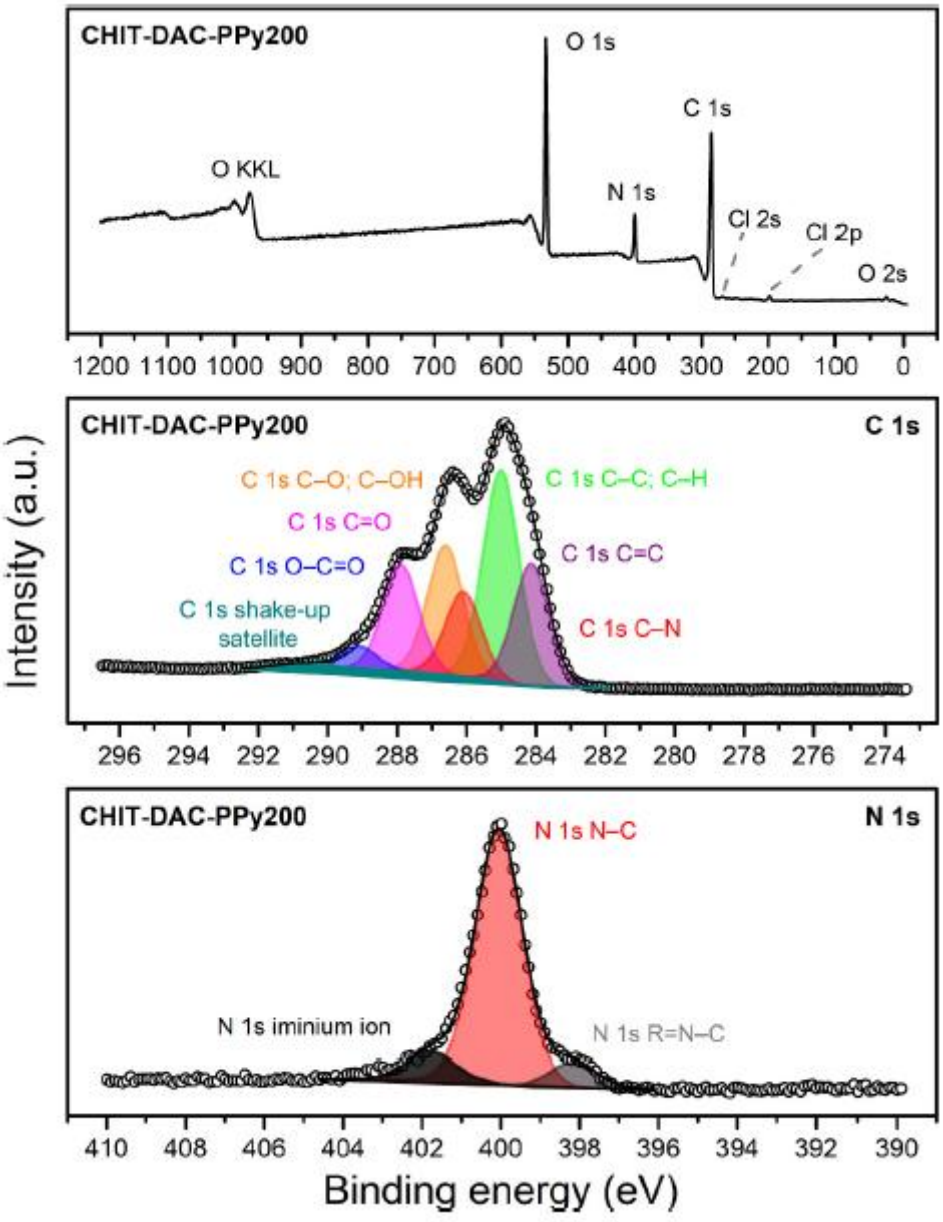

Fig. 4. XPS survey spectrum (top) and high-resolution C 1s (middle) and N 1s (bottom) scans obtained of the $CHIT - DAC - PPy$200 sample.

Subsequently, $CHIT - DAH$, $CHIT - DAAL$, and $CHIT - DADXA$ were used to prepare conjugates analogously to $CHIT - DAC - PPy$200 (see **Fig. 5**). $CHIT - DAH$ and $CHIT - DAAL$ exhibited significantly different behavior during the PPy growth phase (oxidation step) compared to $CHIT - DAC$ and $CHIT - DADXA$. Instead of PPy growing exclusively on the $CHIT - DAP$ conjugate surface, $CHIT - DAH$ and $CHIT - DAAL$ substrates triggered the formation of colloidal PPy particles in the reaction medium, as indicated by the dark color of reaction mixtures after 4 h (see the inset photographs in **Fig. 5**). This behavior can be explained by ionic binding of negatively charged DAH or $DAAL$ macromolecules to chitosan. While DAC or $DADXA$ molecules not forming Schiff bases with

chitosan were washed away, the electrostatic interaction of $DAH/DAAL$ with chitosan prevented their complete removal. When the pH of the solution decreased due to $FeCl_3$ addition, carboxyl groups of DAH and $DAAL$ became protonated, causing electrostatic attraction to vanish. Unbound DAH and $DAAL$ molecules were then released into the solution, acting as stabilizers for PPy colloid formation. The ability to prepare stable colloidal PPy particle solutions utilizing selectively oxidized charged polysaccharides is an interesting opportunity for future exploitation. Nevertheless, $CHIT-DAH-PPy200$ and $CHIT-DAAL-PPy200$ composites retained their nanofibrous structure. DAH and $DAAL$ thus successfully bound to the nanofibers and form a protective DAP layer around $CHITs$ similarly as DAC and $DADXA$, enabling conjugation with py and subsequent PPy growth on their surface (see SEM and TEM micrographs in **Fig. 5**). IR spectra of the prepared composites confirmed the presence of PPy, manifested by absorption bands at around 1550 and 790 cm^{-1}.

Next, conductivity was measured for neat $CHITs$, bulk samples of $CHIT-DAC-PPy200$ and $CHIT-DAAL-PPy200$ prepared for this purpose, as described in Section 2.4. While the specific conductivity of neat $CHITs$ was barely measurable (0.23 nS/cm), the specific conductivities of the PPy samples were 23 and 13 μS/cm, respectively — five orders of magnitude higher. The lower conductivity of $CHIT-DAAL-PPy200$ likely results from reduced PPy deposition on the composite, as a portion of the PPy formed a colloid, as noted above. Although the conductivities of $CHIT-DAC-PPy200$ and $CHIT-DAAL-PPy200$ may be insufficient for applications in sensors or capacitors, they are adequate for biological applications, where materials with similar conductivities are used as scaffolds supporting cell growth and proliferation [**33**].

Because one of the potential uses of the prepared conductive composites is in the biomedical field, where they could serve as cellular scaffolds or wound dressings, initial cytotoxicity testing was performed using the NIH/3T3 cell line, as described in Section 2.4. Results of the cytotoxicity tests are summarized in **Fig. 6** and expressed as a reduction in relative cell viability compared to the reference cultivated on tissue culture plastic. Although cell viability in direct contact with $CHITs$ was unaffected, $CHIT-DAC$ had a major effect on cell viability. This is not surprising, as DAC is considered cytotoxic at concentration exceeding 0.5 mg/mL [**25**]. Interestingly, the $CHIT-DAAL$ samples did not significantly impact cell viability. This remarkable result can be attributed to the negative electrostatic charge of the $DAAL$ layer, which repels cells from the highly reactive — CHO groups, whose presence is detrimental to cell viability. Notably, neither $CHIT-DAAL-PPy200$ nor $CHIT-DAC-PPy200$ significantly impacted cell viability. The PPy layer greatly improved the biocompatibility of $CHIT-DAC$. Thus, both composites can be considered non-cytotoxic.

A one-way ANOVA with a post hoc Tukey's Multiple Comparison test ($p < 0.001$) was used to determine the statistical significance of differences in cell viability between the samples. As indicated in **Fig. 6**, $CHIT-DAC$ exhibited a significant decrease in cell viability compared with the reference and all other samples ($p < 0.001$). No significant differences in cell viability were observed between the reference, $CHIT$, $CHIT-DAAL$, $CHIT-DAC-PPy200$, and $CHIT-DAAL-PPy200$. However, further evaluation, such as testing with different cell lines like HaCaT - an aneuploid immortal keratinocyte cell line from adult human skin, will be necessary before these materials can be used in specific applications, such as wound healing.

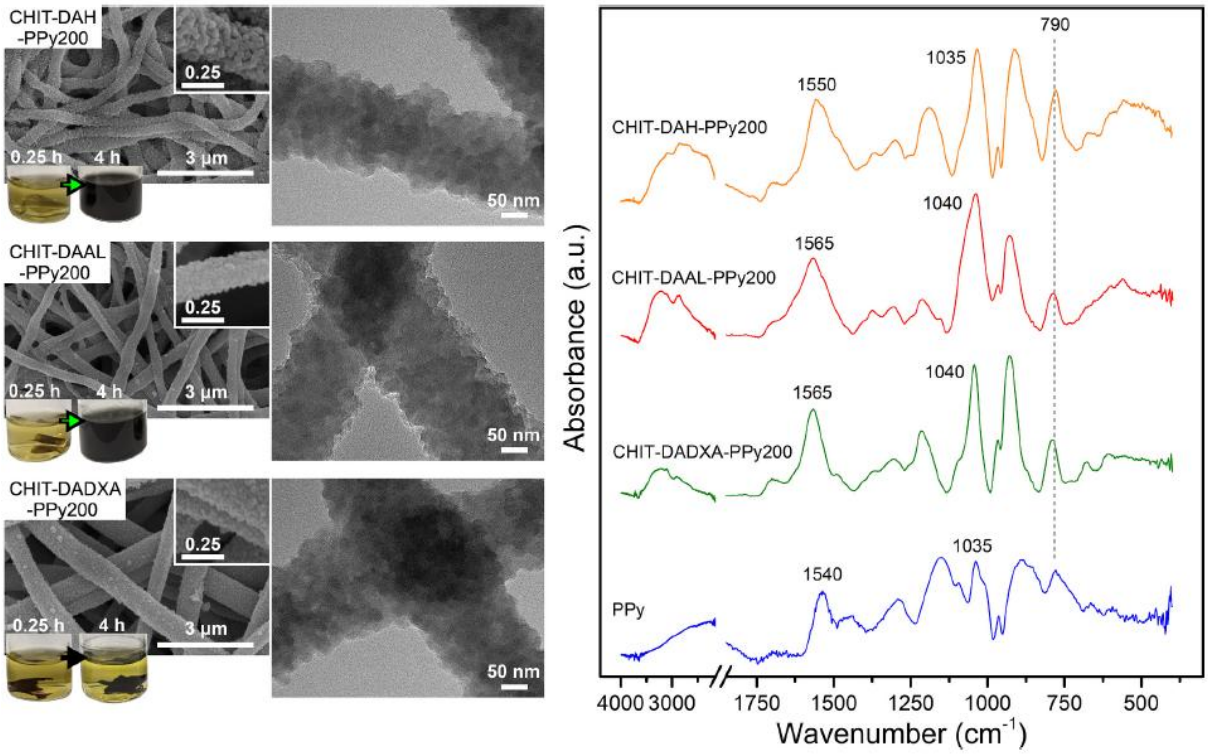

Fig. 5. SEM, TEM, and $FT-IR$ analyses of the prepared $CHIT-DAP$ conjugates with covalently attached PPy.

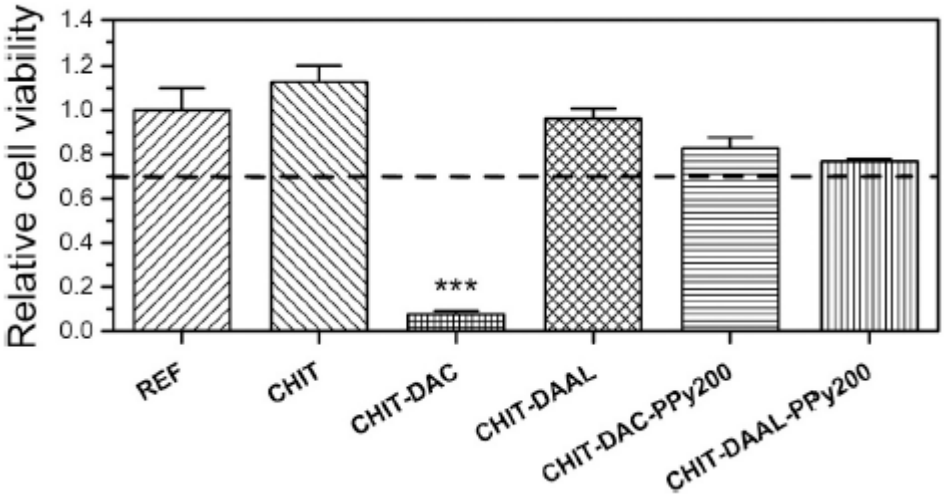

Fig. 6. Cell viability in direct contact with neat $CHITs$, $CHITs$ conjugated with DAC and $DAAL$, and $CHIT-DAAL-PPy200$ and $CHIT-DAC-PPy200$. Data were expressed as mean $\pm$ standard error of the mean ($n = 4$ per group). Statistically significant differences were determined by ANOVA with a post hoc Tukey's Multiple Comparison test; $p < 0.001$. A three-asterisk mark indicates a statistically significant difference compared to the reference.

4. Conclusions

Chitosan nanofibers ($CHITs$) with covalently bound polypyrrole (PPy) have been successfully synthesized using various dialdehyde polysaccharides ($DAPs$). The roles of DAPs in the preparation of these composites are as follows: (i) $DAPs$ undergo a Schiff base reaction with $CHITs$, stabilizing and protecting the nanofibers from harsh conditions during PPy synthesis; (ii) $DAPs$ facilitate the conjugation of pyrrole (py) via an aldol condensation reaction to the surface of $CHIT-DAP$

composites, thereby creating hotspots for subsequent PPy growth. The Schiff base conjugation reaction between $DAPs$ and $CHITs$ and the aldol condensation with py were confirmed by $FT-IR$ analysis and further supported by XPS analysis. Due to the conjugation of py to the $CHIT-DAP$ composites surface, PPy was shown to preferentially grow on their surface up to an n_CHO: $2n_{\mathrm{py}}$ molar ratio. This approach minimizes waste and improves the efficiency of PPy composite production. While all $DAPs$ stabilize $CHITs$ at low pH and facilitate conjugation with py, the charged $DAPs$ (i.e., DAH and $DAAL$) also initiate the formation of PPy colloids. The best results were obtained for composites prepared using DAC and $DADXA$. The prepared materials demonstrated good cytocompatibility, and although their conductivity may not be sufficient for industrial applications, they show promise as scaffolds or wound healing materials in biomedical applications.

The proposed method enables the facile preparation of conductive nanofibrous composites with covalently bound PPy without the need for organic solvents, complex procedures, organic linkers, or toxic reactants. It relies almost exclusively on biopolymers from renewable sources, thereby reducing environmental impact. This procedure may be also applicable to other amine-containing polymer substrates, further expanding the possibilities for the preparation of new PPy composites.

References

[1] J. Huang, J. Li, X. Xu, L. Hua, Z. Lu, In situ loading of Polypyrrole onto aramid nanofiber and carbon nanotube aerogel fibers as physiology and motion sensors, ACS Nano 16 (2022) 8161-8171, **https://doi.org/10.1021/acsnano.2c01540**.

[2] Y. Li, Y. Gao, L. Lan, Q. Zhang, L. Wei, M. Shan, L. Guo, F. Wang, J. Mao, Z. Zhang, L. Wang, Ultrastretchable and wearable conductive multifilament enabled by buckled polypyrrole structure in parallel, Npj Flex. Electron. 6 (2022) 42, **https:// doi.org/10.1038/s41528-022-00176-6**.

[3] U.D. Chavan, P. Prajith, B. Kandasubramanian, Polypyrrole based cathode material for battery application, Chem. Eng. J. Adv. 12 (2022) 100416, **https://doi.org/ 10.1016/j.ceja.2022.100416**.

[4] R. Guo, W. Guo, H. Pei, B. Wang, X. Guo, N. Liu, Z. Mo, Polypyrrole deposited electrospun PAN/PEI nanofiber membrane designed for high efficient adsorption of chromium ions (VI) in aqueous solution, Colloids Surf. A Physicochem. Eng. Asp. 627 (2021) 127183, **https://doi.org/10.1016/j.colsurfa.2021.127183**.

[5] K. Skopalová, K.A. Radaszkiewicz, V. Kašpárková, J. Stejskal, P. Bober, I. Junkar, M. Mozetič, Z. Capáková, M. Lehocký, M. Kašparová, J. Pacherník, P. Humpolíček, Modulation of differentiation of embryonic stem cells by Polypyrrole: the impact on neurogenesis, Int. J. Mol. Sci. 22 (2021) 501, **https://doi.org/10.3390/ ijms22020501**.

[6] P. Humpolíček, V. Kašpárková, J. Pacherník, J. Stejskal, P. Bober, Z. Capáková, K. A. Radaszkiewicz, I. Junkar, M. Lehocký, The biocompatibility of polyaniline and polypyrrole: a comparative study of their cytotoxicity, embryotoxicity and impurity profile, Mater. Sci. Eng. C 91 (2018) 303-310, **https://doi.org/10.1016/). msec.2018.05.037**.

[7] M.H.R. Borges, B.E. Nagay, R.C. Costa, J.G.S. Souza, M.T. Mathew, V.A.R. Barao, Recent advances of polypyrrole conducting polymer film for biomedical application: toward a viable

platform for cell-microbial interactions, Adv. Colloid Interface Sci. 314 (2023) 102860, **https://doi.org/10.1016/j.cis.2023.102860**.

[8] L. Mahelová, P. Slobodian, K. Kocourková, A. Minařík, R. Moučka, M. Trchová, M. Martínková, K. Skopalová, Z. Víchová, V. Kašpárková, P. Humpolíček, Method for in situ polypyrrole coating, and the example of its use for functionalization of polyurethane anisotropic electrospun mats, Heliyon 10 (2024) e27883, **https://doi. org/10.1016/j.heliyon.2024.e27883**.

[9] T.V. Vernitskaya, O.N. Efimov, Polypyrrole: a conducting polymer; its synthesis, properties and applications, Russ. Chem. Rev. 66 (1997) 443-457, **https://doi.org/ 10.1070/RC1997v066n05ABEH000261**.

[10] S. Káčerová, Z. Víchová, K. Valášková, J. Vícha, L. Münster, V. Kašpárková, O. Vašíček, P. Humpolíček, Biocompatibility of colloidal polypyrrole, Colloids Surf. B Biointerfaces 232 (2023) 113605, **https://doi.org/10.1016/j. colsurfb.2023.113605**.

[11] R. Cruz-Silva, E. Amaro, A. Escamilla, M.E. Nicho, S. Sepulveda-Guzman, L. Arizmendi, J. Romero-Garcia, F.F. Castillon-Barraza, M.H. Farias, Biocatalytic synthesis of polypyrrole powder, colloids, and films using horseradish peroxidase, J. Colloid Interface Sci. 328 (2008) 263-269, **https://doi.org/10.1016/j. jcis.2008.09.021**.

[12] L.-X. Wang, X.-G. Li, Y.-L. Yang, Preparation, properties and applications of polypyrroles, React. Funct. Polym. 47 (2001) 125-139, **https://doi.org/10.1016/ S1381-5148(00)00079-1**.

[13] J. Upadhyay, A. Kumar, K. Gupta, M. Mandal, Investigation of physical and biological properties of polypyrrole nanotubes-chitosan nanocomposites, Carbohydr. Polym. 132 (2015) 481-489, **https://doi.org/10.1016/j. carbpol.2015.06.028**.

[14] K. Abu-Rabeah, B. Polyak, R.E. Ionescu, S. Cosnier, R.S. Marks, Synthesis and characterization of a pyrrole—alginate conjugate and its application in a biosensor construction, Biomacromolecules 6 (2005) 3313-3318, **https://doi.org/10.1021/bm050339j**.

[15] J. Yang, G. Choe, S. Yang, H. Jo, J.Y. Lee, Polypyrrole-incorporated conductive hyaluronic acid hydrogels, Biomater. Res. 20 (2016) 31, **https://doi.org/10.1186/ s40824-016-0078-y**.

[16] S. Káčerová, M. Muchová, H. Doudová, L. Münster, B. Hanulíková, K. Valášková, V. Kašpárková, Kuřitka, P. Humpolíček, Z. Víchová, O. Vašíček, J. Vícha, Chitosan/dialdehyde cellulose hydrogels with covalently anchored polypyrrole: novel conductive, antibacterial, antioxidant, immunomodulatory, and antiinflammatory materials, Carbohydr. Polym. 327 (2024) 121640, **https://doi.org/ 10.1016/j.carbpol.2023.121640**.

[17] S. Koprivica, M. Siller, T. Hosoya, W. Roggenstein, T. Rosenau, A. Potthast, Regeneration of aqueous periodate solutions by ozone treatment: a sustainable approach for dialdehyde cellulose production, ChemSusChem 9 (2016) 825-833, **https://doi.org/10.1002/cssc.201501639**.

[18] M. Muchová, L. Münster, Z. Capáková, V. Mikulcová, I. Kuřitka, J. Vícha, Design of dialdehyde cellulose crosslinked poly(vinyl alcohol) hydrogels for transdermal drug delivery and wound dressings, Mater. Sci. Eng. C 116 (2020) 111242, **https:// doi.org/10.1016/j.msec.2020.111242**.

[19] K.Y. Lee, D.J. Mooney, Alginate: properties and biomedical applications, Prog. Polym. Sci. 37 (2012) 106-126, **https://doi.org/10.1016/j. progpolymsci.2011.06.003**.

[20] A. Usman, M.T. Hussain, N. Akram, M. Zuber, S. Sultana, W. Aftab, K.M. Zia, M. Maqbool, Y.M. Alanazi, A. Nazir, M.A. Javaid, Modulating alginate-polyurethane elastomer properties: influence of NCO/OH ratio with aliphatic diisocyanate, Int. J. Biol. Macromol. 278 (2024) 134657, **https://doi.org/10.1016/ j.ijbiomac.2024.134657**.

[21] M.A. Javaid, Y.M. Alanazi, D. Li, Y. Gong, M. El-Harbawi, S. Ahmad, U. Tahir, I. Ullah, M.T. Hussain, H. Iqbal, Synthesis and optimization of molecular weight of chitosan and carboxymethyl cellulose based polyurethanes, Int. J. Biol. Macromol. 281 (2024) 135709, **https://doi.org/10.1016/j.ijbiomac.2024.135709**.

[22] J.R.E. Fraser, T.C. Laurent, U.B.G. Laurent, Hyaluronan: its nature, distribution, functions and turnover, J. Intern. Med. 242 (1997) 27-33, **https://doi.org/10.1046/j.1365-2796.1997.00170.x**.

[23] G. Sun, J.J. Mao, Engineering dextran-based scaffolds for drug delivery and tissue repair, Nanomed 7 (2012) 1771-1784, **https://doi.org/10.2217/nnm.12.149**.

[24] A. Důbravová, M. MuchovÁ, D. škoda, L. Lovecká, L. Simoníková, I. Kuřitka, J. Vícha, L. Münster, Highly efficient affinity anchoring of gold nanoparticles on chitosan nanofibers via dialdehyde cellulose for reusable catalytic devices, Carbohydr. Polym. 323 (2024) 121435, **https://doi.org/10.1016/j. carbpol.2023.121435**.

[25] M. Muchová, L. Münster, A. Vávrová, Z. Capáková, I. Kuřitka, J. Vícha, Comparison of dialdehyde polysaccharides as crosslinkers for hydrogels: the case of poly(vinyl alcohol), Carbohydr. Polym. 279 (2022) 119022, **https://doi.org/10.1016/j. carbpol.2021.119022**.

[26] L. Münster, J. Vícha, J. Klofáč, M. Masař, P. Kucharczyk, I. Kuřitka, Stability and aging of solubilized dialdehyde cellulose, Cellulose 24 (2017) 2753-2766, **https:// doi.org/10.1007/s10570-017-1314-x**.

[27] L. Münster, M. Fojtů, Z. Capáková, M. Muchová, L. Musilová, T. Vaculovič, J. Balvan, I. Kuřitka, M. Masařík, J. Vícha, Oxidized polysaccharides for anticancer-drug delivery: what is the role of structure? Carbohydr. Polym. 257 (2021) 117562 **https://doi.org/10.1016/j.carbpol.2020.117562**.

[28] S. Veelaert, D. De Wit, K.F. Gotlieb, R. Verheá, Chemical and physical transitions of periodate oxidized potato starch in water, Carbohydr. Polym. 33 (1997) 153-162, **https://doi.org/10.1016/S0144-8617(97)00046-5**.

[29] M.R. Kasaai, Determination of the degree of N-acetylation for chitin and chitosan by various NMR spectroscopy techniques: a review, Carbohydr. Polym. 79 (2010) 801-810, **https://doi.org/10.1016/j.carbpol.2009.10.051**.

[30] K.A. Kristiansen, A. Potthast, B.E. Christensen, Periodate oxidation of polysaccharides for modification of chemical and physical properties, Carbohydr. Res. 345 (2010) 1264-1271, **https://doi.org/10.1016/j.carres.2010.02.011**.

[31] L. Münster, Z. Capáková, P. Humpolíček, I. Kuřitka, B.E. Christensen, J. Vícha, Dicarboxylated hyaluronate: synthesis of a new, highly functionalized and biocompatible derivative, Carbohydr. Polym. 292 (2022) 119661, **https://doi.org/ 10.1016/j.carbpol.2022.119661**.

[32] L. Münster, M. Fojtů, M. Muchová, F. Latečka, S. Káčerová, Z. Capáková, T. Juriňáková, I. Kuřitka, M. Masařík, J. Vícha, Enhancing cisplatin anticancer effectivity and migrastatic potential by modulation of molecular weight of oxidized dextran carrier, Carbohydr. Polym. 272 (2021) 118461, **https://doi.org/10.1016/j. carbpol.2021.118461**.

[33] Y. Liang, J.C.-H. Goh, Polypyrrole-incorporated conducting constructs for tissue engineering applications: a review, Bioelectricity 2 (2020) 101-119, **https://doi. org/10.1089/bioe.2020.0010**.